International Journal of Research
Available at https://edupediapublications.org/journals
p-ISSN: 2348-6848
e-ISSN: 2348-795X
Volume 03 Issue 18
December 2016

Color Attenuation Prior for Removing the Haze in Single Image

[1] Vempalaku Priyanka & [2] T.Ravi Kumar

[1] M.Tech., Department of ECE (DECS),Dr.K.V.Subba Reddy college of Engineering for Women, Email.Id- vempalakupriyanka12@gmail.com, Kurnool.

[2] Assistant Professor, Department of ECE (DECS)Dr.K.V.Subba Reddy college of Engineering for Women,Guide Email id- ravi3922@gmail.com, Kurnool.

ABSTRACT

Single image haze removal has been a challenging problem due to its ill-posed nature. In this paper, we propose a simple but powerful color attenuation prior for haze removal from a single input hazy image. By creating a linear model for modeling the scene depth of the hazy image under this novel prior and learning the parameters of the model with a supervised learning method, the depth information can be well recovered. With the depth map of the hazy image, we can easily estimate the transmission and restore the scene radiance via the atmospheric scattering model, and thus effectively remove the haze from a single image. Experimental results show that the proposed approach outperforms state-of-the-art haze removal algorithmsin terms of both efficiency and the dehazing effect.

INTRODUCTION TO HAZY IMAGES

Open air pictures taken in terrible climate (e.g., foggy or cloudy) for the most part lose complexity and devotion, coming about because of the way that light is assimilated and scattered by the turbid medium, for example, particles and water beads in the environment amid the procedure of engendering. Additionally, most programmed frameworks, which firmly rely on upon the meaning of the info pictures, neglect to work ordinarily brought about by the corrupted pictures. In this manner, enhancing the system of picture fog expulsion will profit many picture comprehension and PC vision applications, for example, aeronautical symbolism [1], picture characterization [2]–[5], picture/video recovery

[6]–[8], remote detecting [9]–[11] and video investigation and acknowledgment [12]–[14].

Since centralization of the murkiness is not quite the same as place to place and it is difficult to recognize in a foggy picture, picture dehazing is subsequently a testing undertaking. Early specialists utilize the conventional procedures of picture processing to expel the dimness from a solitary picture (for example, histogram-based dehazing strategies [15]–[17]). Be that as it may, the dehazing impact is constrained, in light of the fact that a solitary foggy picture can scarcely give much data. Later, specialists attempt to enhance the dehazing execution with numerous pictures. In [18]–[20], polarization based strategies are utilized for dehazing with various pictures which are brought with various degrees of polarization. In [21]–[23], Narasimhan et al. propose fog expulsion approaches with numerous pictures of a similar scene under various climate conditions. In [24] and [25], dehazing is led in view of the given profundity data.

As of late, huge advance has been made in single picture dehazing in view of the physical model. Under theassumption that the

neighborhood complexity of the fog free picture is much higher than that in the murky picture, Tan [26] proposes a novel dimness expulsion strategy by augmenting the nearby differentiation of the picture in view of Markov Random Field (MRF). Albeit Tan's approach can accomplish great outcomes, it tends to create over-immersed pictures. Fattal [27] proposes to expel the fog from shading pictures in light of Independent Component Analysis (ICA), yet the approach is tedious and can't be utilized for grayscale picture dehazing. Besides, it has a few troubles to manage thick dimness pictures. Motivated by the generally utilized dull question subtraction system [28] and in view of a substantial number of examinations on dimness free pictures, He et al. [29] find the dull channel earlier (DCP) that, in the greater part of the non-sky patches, no less than one shading channel has a few pixels whose powers are low and near zero. With this earlier, they appraise the thickness of cloudiness, and reestablish the murkiness free picture by the air disseminating model. The DCP approach is straightforward and powerful by and large. Be that as it may, it can't well handle the sky pictures and is computationally escalated. Some enhanced calculations [30]–[36], [45]–[51] are proposed to beat the shortcoming of the DCP approach. For effectiveness, Gibson et al. [31], Yu et al. [32], He et al. [43], Tarel and Hautiere [45], and Tarel et al. [46] supplant the tedious delicate tangling [44] with standard middle sifting, "middle of middle channel", guided joint two-sided separating [37]–[42] and guided picture separating, individually. As far as dehazing quality, Kratz and Nishino [48] and Nishino et al. [49] show the picture with a factorial Markov irregular documented to appraise the scene brilliance all the more precisely; Meng et al. [50] propose a compelling regularization dehazing strategy to reestablish the murkiness free picture by investigating the inborn limit limitation; Tang et al. [51] consolidate

Fig.1. An overview of the proposed dehazing method. Top-left: Input hazy image. Top-right: Restored depth map. Bottom-left: Restored transmission map. Bottom-right: Dehazed image.

four types of haze-relevant features with Random Forest [52] to estimate the transmission. Despite the remarkable progress, the limitation of the state-of-the-art methods

lies in the fact that the haze-relevant priors or heuristic cues used are not effective or efficient enough.In this paper, we propose a novel color attenuation prior for single image dehazing. This simple and powerful prior can help to create a linear model for the scene depth of the hazy image. By learning the parameters of the linear model with a supervised learning method, the bridge between the hazy image and its corresponding depth map is built effectively. With the recovered depth information, we can easily remove the haze from a single hazy image. An overview of the proposed dehazing method is shown in Figure 1. The efficiency of this dehazing method is dramatically high and the dehazing effectiveness is also superior to that of prevailing dehazing algorithms as we will show in Section VI. A conference version of our work has been presented in [53].

The remainder of this paper is organized as follows: In Section II, we review the atmospheric scattering model which is widely used for image dehazing and give a concise analysis on the parameters of this model. In Section III, we present a novel color attenuation prior. In Section IV, we discuss the approach of recovering the scene depth with the proposed color attenuation prior. In Section V, the method of image dehazing with the depth information is described. In Section VI, we present and analyze the experimental results. Finally, we summarize this paper in Section VII.

AN IMPROVED FOG-REMOVING METHOD

2.1. The Retinex algorithm.

Retinex algorithm [2, 3] has showed good effect on removing fog from image. Retinex algorithm is to reduce the effects of incident light on the image, and to strengthen the reflection image as follows:

$$R_I\{x,y) = \log I_i\ (x,y) - \log [F(x,y) * I_i(x,y)] \quad I = 1, \cdots, n \qquad (1)$$

Rl(x,y) is the output corresponding to the L channel, II (x, y) is an input luminance image pixel value of the L channel, the parameter * is the convolution operation, the parameter n in the color channel number, F (x, y) represents the center / surround function, it is represented by Gauss function as formulation (2).

$$F(x,y) = Ke^{-(x^2+y^2)/\sigma^2} \qquad (2)$$

The parameter (j controls center / surround function range, the value is smaller, the center / surround function is sharper.

The wavelet transform algorithm.

2-D discrete wavelet transform algorithm is a well-known method for image processing. It use high-pass filter and lowpass filter two times respectively at horizontal and vertical direction, the decomposition results are as follows: the approximate component A, the level of detail components H, vertical detail coefficients V and diagonal detail component D. Approximate coefficients represent the background picture which has the lowest frequency, detail coefficient represents the scene information which has the high frequency.

The imporved fog-removing method

Retinex algorithm can enhance most of the information of image, however but since it just increases the overall outline, the details of the image are not outstanding. On the other hand, wavelet image enhancement by suppressing

low frequency information of the image and enhanced image of high frequency information so as to enhance image details and outline of the image noise reduction at the same time.We propose an improved fog-removing method which has combined the merits of Retinex algorithm and Wavelet transform algorithm, this improved fog-removing method firstly use Retinex algorithm to enhance overall outline information of the image; then use wavelet image enhancement method to get high frequency information from the Retinex-ed image, finally a more clearly and fog-removed image can be obtained. We named this improved method as R + WT algorithm.

The steps of the R+WT method are as follows:
(a) Input the fog-image.
(b) Put the above fog-image into logarithm domain.
(c) To obtain the result image R(x,y) by using the above formulation (1) and (2).
(d) By using a linear stretch processing to make the above R(x,y) image size to be similar with the original image.
(e) Using wavelet transform method decomposed R(x,y) image into two layers.
(f) Then to increase the high frequency and suppress low frequency of the image from step (e).
(g) Output the result fog removed image.

Comparison with other state of art image processing techniques[7]

In order to analyze the advantages of the Retinex image enhancement techniques, we compare the retinex result with other image enhancement techniques, including auto gain/offset, gama correction, histogram equalization and homomorphic filtering. As a result, all the other techniques heavily depend on input images. For auto gain/offset, it could achieve dynamic range compression but at the loss of details due to saturation and clipping. For gama correction, it is good to improve pictures either too dark or too bright but it is a global function applied to the picture, thus there is no details enhancement involved. For histogram equalization and homomorphic filtering, they all failed for bi-modal pictures, which includes the information both dark and bright areas. (As Fig.8 but they all could achieve some better effect for Fig.9 since the picture is in a general dark situation. But for retinex, it could achieve satisfactory results for both pictures, thus its benefits are obviously to see.

Multiscale retinex is an effective algorithm of retinex. It can have dynamic range compression and color rendition effects at the same time. For color images, color restoration is necessary in the case that the three-color channels are not intensity balanced. The gain/offset processes are used to shift, compress and clip the output of MSRCR to the display domain, which will improve the contrast. And one of the important characteristics of MSRCR with gain/offset algorithms is “canonical”, which means that the parameters of number of scales, scales, gain and offsets do not vary from image to image or between band to band.
As compared with other image enhancement techniques, the Retinex enhancement has the following advantage: 1. “Canonical” constant – once it is defined, image enhancement is an automatic process independent of inputs; 2. Has general application on all pictures; 3. Good dynamic range compression and color rendition effect.
For the future work, the color image should be further analyzed. Study the chapter 6 of the textbook “Digital Image Processing”, try to analyze the color model suitable for the retinex enhancement to improve the color correction function (Ci(x,y)) to achieve the better color rendition, at the same time, the empirical values of gain (G), offset (b) could also be improved.

International Journal of Research
Available at https://edupediapublications.org/journals
p-ISSN: 2348-6848
e-ISSN: 2348-795X
Volume 03 Issue 18
December 2016

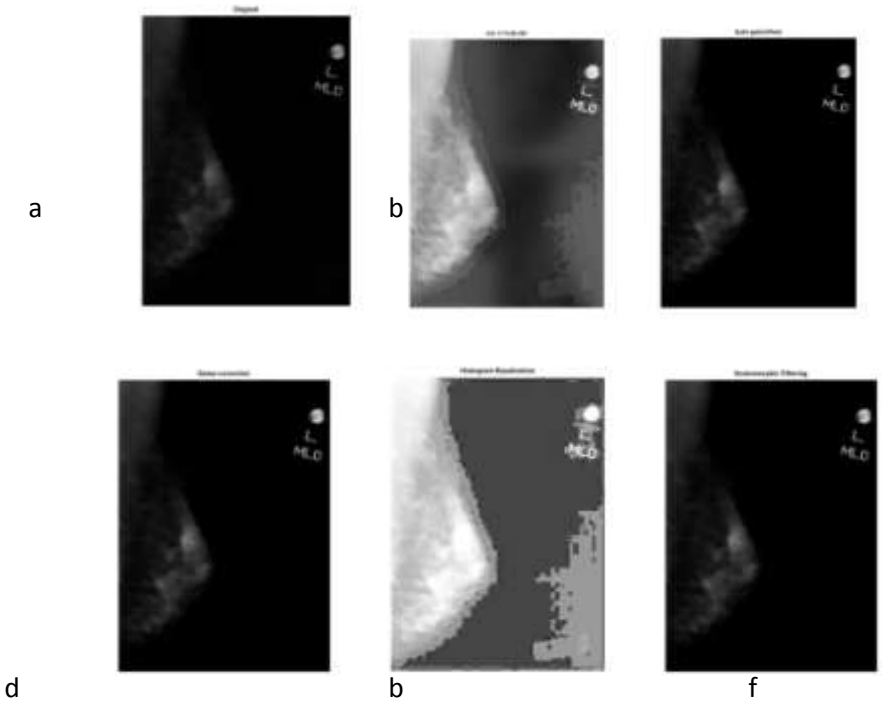

Fig. 5 Comparison of Retinex with other techniques (Example 1)a)original image b) Retinex enhanced image c) Auto gain/offset d) Gama Correction e) Histogram equalization; f)Homomorphic filtering

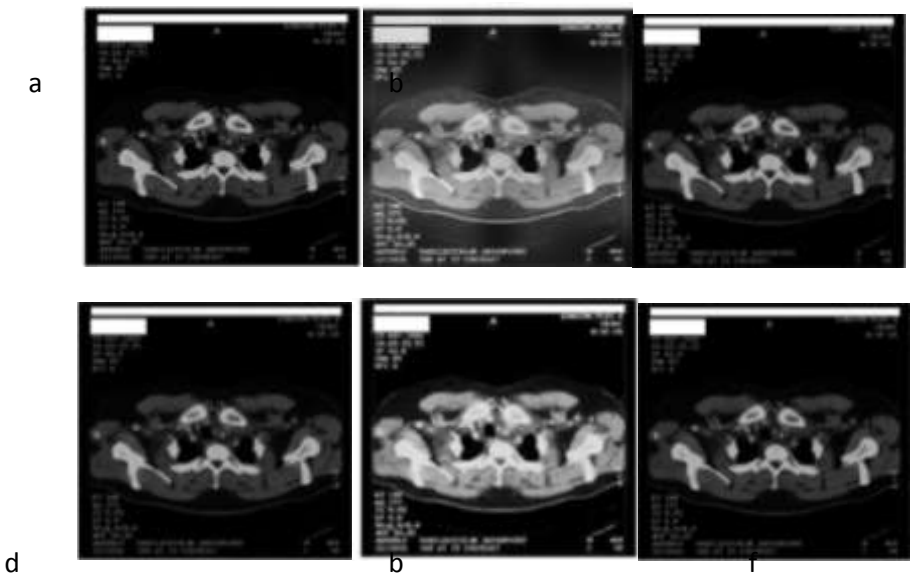

Fig. 6 Comparison of Retinex with other techniques (Example 2)

original image b) Retinex enhanced image c) Auto gain/offset d) Gama Correction e) Histogram equalization; f)Homomorphic filtering

COLOR ATTENUATION PRIOR

To detect or remove the haze from a single image is a challenging task in computer vision, because little information about the scene structure is available. In spite of this,Fig. 2. The concentration of the haze is positively correlated with the difference between the brightness and the saturation. (a) A hazy image.(b) The close-up patch of a dense-haze region and its histogram. (c) The close-up patch of a moderately hazy region and its histogram. (d) The close-up patch of a haze-free region and its histogram.

the human brain can quickly identify the hazy area from the natural scenery without any additional information. This inspired us to conduct a large number of experiments on various hazy images to find the statistics and seek a new prior for single image dehazing. Interestingly, we find that the brightness and the saturation of pixels in a hazy image vary sharply along with the change of the haze concentration. Figure 2 gives an example with a natural scene to show how the brightness and the saturation of pixels vary within a hazy image. As illustrated in Figure 2(d), in a haze-free region, the saturation of the scene is pretty high, the brightness is moderate and the difference between the brightness and the saturation is close to zero. But it is observed from Figure 2(c) that the saturation of the patch decreases sharply while the color of the scene fades under the influence of the haze, and the brightness increases at the same time producing the high value of the difference. Furthermore, Figure 2(b) shows that in a dense-haze region, it is more difficult for us to recognize the inherent color of the scene, and the difference is even higher than that in Figure 2(c). It seems that the three properties (the brightness, the saturation and the difference) are prone to vary regularly in a single hazy image according to this observation. Is this coincidence, or is there a fundamental reason behind this? To answer this question, we first review the process of imaging.

Figure 3 illustrates the imaging process. In the haze-free condition, the scene element reflects the energy that is fromthe illumination source (e.g., direct sunlight, diffuse skylight and light reflected by the ground), and little energy is lost when it reaches the imaging system. The imaging system collects the incoming energy reflected from the scene element and focuses it onto the image plane. Without the influence of the haze, outdoor images are usually with vivid color (see Figure 3(a)). In hazy weather, in contrast, the situation becomes more complex (see Figure 3(b)). There are two mechanisms (the direct attenuation and the airlight) in imaging under

hazy weather [23]. On one hand, the direct attenuation caused by the reduction in reflected energy leads to low intensity of the brightness. To understand this, we review the atmospheric scattering model. The term $\mathbf{J}(x)t(x)$ in Equation (1) is used for describing the direct attenuation. It reveals the fact that the intensity of the pixels within the image will decrease in a multiplicative manner. So it turns out that the brightness tends to decrease under the influence of the direct attenuation. On the other hand, the white or gray airlight, which is formed by the scattering of the environmental illumination, enhances the brightness and reduces the saturation. We can also explain this by the atmospheric scatter model. The rightmost term $\mathbf{A}(1-t(x))$ in Equation (1) represents the effect of the airlight. It can be deduced from this term that the effect of the white or gray air light on the observed values is additive. Thus, caused by the air light, the brightness is increased while

International Journal of Research
Available at https://edupediapublications.org/journals
p-ISSN: 2348-6848
e-ISSN: 2348-795X
Volume 03 Issue 18
December 2016

the saturation is decreased. Since the air light plays a more important role in most cases, hazy regions in the image are characterized by high brightness and low saturation. What's more, the denser the haze is, the stronger the influence of the air light would be. This allows us to utilize the difference between the brightness and the saturation to estimate the concentration of the haze. In Figure 4, we show that the difference increases along with the concentration of the haze in a hazy image, as we expected.Since the concentration of the haze increases along with the change of the scene depth in general, we can make an assumption that the depth of the scene is positively correlated with the concentration of the haze and we have: where *d*is the scene depth, *c* is the concentration of the haze, *v* is the brightness of the scene and *s* is the saturation. We regard this statistics as color attenuation prior. Figure 5 gives the geometric description of the color attenuation prior through the HSV color model. Figure 5(a) is the HSV color model, and Figure 5(b-d) are the near, moderate-distance and far scene depths, respectively. Vector **I** indicates the hazy image, passing through the origin and performing the projection of the vector **I** onto a horizontal plane Setting the angle between vector **I** and its projection as α, according to the HSV color model, when α varies between 0 and 90 degrees, the higher the value of α is, the higher the value of tangent α is, which indicates the greater the difference between the component of **I** in the direction of **V** and the component of **I** in the direction of **S**. As the depth increases, the value *v* increases and the saturation ***s*** decreases, and therefore α increases. In other words, the angle α is positively correlated with the depth.

It is worth to point out that Equation (7) is just an intuitional result of the observation and it cannot be an accurate expression about the links among *d*, *v* and *s*. We will find the way to create a more robust expression in the following sections.

SCENE DEPTH RESTORATION

The Linear Model Definition

As the difference between the brightness and the saturation can approximately represent the concentration of the haze,

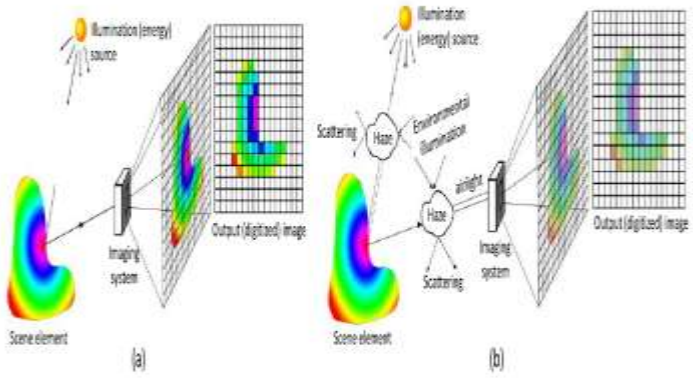

Fig. 3. The process of imaging under different weather conditions. (a) The process of imaging in sunny weather. (b) The process of imaging in hazy weather.

International Journal of Research
Available at https://edupediapublications.org/journals
p-ISSN: 2348-6848
e-ISSN: 2348-795X
Volume 03 Issue 18
December 2016

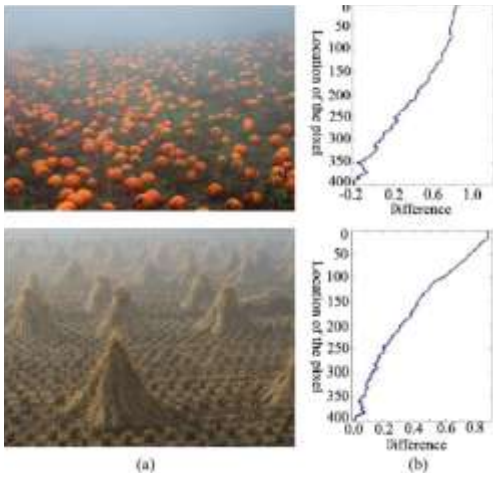

Fig. 4. Difference between brightness and saturation increases along with the concentration of the haze. (a) A hazy image. (b) Difference between brightness and saturation.

Training Data Collection

In order to learn the coefficients θ_0, θ_1 and θ_2 accurately, the training data are necessary. In our case, a training sample consists of a hazy image and its corresponding ground truth depth map. Unfortunately, the depth map is very difficult to obtain due to the fact that there is no reliable means to measure the depths in outdoor scenes. Current depth cameras such as Kinect are not able to acquire the accurate depth information.Inspired by Tang et al.'s method for preparing the training data [51], we collect the haze-free images from Google Images and Flickr and use them to produce the synthetic depth maps and the corresponding hazy images for obtaining enough training samples. The process of generating the training samples is illustrated in Figure 7. Firstly, for each haze-free image, we generate a random depth map with the same size. The values of the pixels within the synthetic depth map are drawn from the standard uniform distribution on the open interval (0, 1). Secondly, we generate the random atmospheric light **A** (*k*, *k*, *k*) where the value of *k* is between 0.85 and 1.0. Finally, we generate the hazy image **I** with the random depth map *d* and the random atmospheric light **A** according to Equation (1) and Equation (2). In our case, 500 haze-free images are used for generating the training samples (500 random depth maps and 500 synthetic hazy images).

Learning Strategy

What we are interested in is the joint conditional concentration:

$$L = p(d(x_1), \ldots, d(x_n) | x_1, \ldots, x_n, \theta_0, \theta_1, \theta_2, \sigma^2), \quad (11)$$

where*n* is the total number of pixels within the training hazy images, $d(x_n)$ is the depth of the nth scene point, and L is the likelihood. Assuming that the random error at each scene point is independent (i.e. $p(\varepsilon_1,\ldots, \varepsilon_n) = \prod_{i=1,\ldots,n} p(\varepsilon_i)$), we can rewrite Equation (11) as:

International Journal of Research
Available at https://edupediapublications.org/journals
p-ISSN: 2348-6848
e-ISSN: 2348-795X
Volume 03 Issue 18
December 2016

$$L = \prod_{i=1}^{n} p(d(x_i)|x_i, \theta_0, \theta_1, \theta_2, \sigma^2). \qquad (12)$$

According to Equation (9) and Equation (12), we have:

$$L = \prod_{i=1}^{n} \frac{1}{\sqrt{2\pi\sigma^2}} e^{-\frac{dg_i - (\theta_0 + \theta_1 v(x_i) + \theta_2 s(x_i))}{2\sigma^2}}, \qquad (13)$$

where dg_i represents the ground truth depth of the ith scene point. So the problem is to find the optimal values of θ_0, θ_1, θ_2, and σ to maximum L. For convenience, instead of maximizing the likelihood directly, we maximize the natural logarithm of the likelihood ln L. Therefore, the problem can be expressed as follows:

$$\arg\max_{\theta_0,\theta_1,\theta_2,\sigma} \ln L = \sum_{i=1}^{n} \ln\left(\frac{1}{\sqrt{2\pi\sigma^2}} e^{-\frac{dg_i - (\theta_0 + \theta_1 v(x_i) + \theta_2 s(x_i))}{2\sigma^2}}\right). \qquad (14)$$

To solve the problem, we first calculate the partial derivative of ln L with respect to σ and make it equal to zero:

$$\frac{\partial \ln L}{\partial \sigma} = -\frac{n}{\sigma} + \frac{1}{\sigma^3} \sum_{i=1}^{n} (dg_i - (\theta_0 + \theta_1 v(x_i) + \theta_2 s(x_i))) = 0. \qquad (15)$$

According to Equation (15), the maximum likelihood estimate for the variable σ^2 is:

$$\sigma^2 = \frac{1}{n} \sum_{i=1}^{n} (dg_i - (\theta_0 + \theta_1 v(x_i) + \theta_2 s(x_i)))^2. \qquad (16)$$

As for the linear coefficients θ_0, θ_1 and θ_2, we use the gradient descent algorithm to estimate their values. By taking the partial derivatives of ln L with respect to θ_0, θ_1 and θ_2 respectively,

Algorithm 1 Parameters Estimation

Input: the training brightness vector v, the training saturation vector s, the training depth vector d, and the number of iterations t
Output: linear coefficients θ_0, θ_1, θ_2, the variable σ^2
Auxiliary functions:
function for obtaining the size of the vector: $n = size(in)$
function for calculating the square: $out = square(in)$
Begin

```
n = size(v);
θ0 = 0; θ1 = 1; θ2 = -1;
sum = 0; wSum = 0; vSum = 0; sSum = 0;
for iteration from 1 to t do
    for index from 1 to n do
        temp = d[i] - θ0 - θ1 * v[i] - θ2 * s[i];
        wSum = wSum + temp;
        vSum = vSum + v[i] * temp;
        sSum = sSum + s[i] * temp;
        sum = sum + square(temp);
    end for
    σ^2 = sum / n;
    θ0 = θ0 + wSum; θ1 = θ1 + vSum; θ2 = θ2 + sSum;
end for
```

End

International Journal of Research
Available at https://edupediapublications.org/journals
p-ISSN: 2348-6848
e-ISSN: 2348-795X
Volume 03 Issue 18
December 2016

It is significant that the expression above is utilized for repeating progressively, and the documentation: = does not expressthe scientific uniformity, but rather implies that setting the estimation of θi in the left term to be the estimation of the correct term. The method for taking in the direct coefficients θ0, θ1, θ2 and the variable σ2is appeared in Algorithm 1.

We utilized 500 preparing tests containing 120 million scene focuses to prepare our straight model. There are 517 ages for our situation, and the best learning outcome is that θ0= 0.121779, θ1= 0.959710, θ2= −0.780245, σ = 0.041337. Once the estimations of the coefficients have been resolved, they can be utilized for any single murky picture. These parameters will be utilized for reestablishing the scene profundities of the murky pictures in this paper. β = 1.2

EXPERIMENTS

In order to verify the effectiveness of the proposed dehazing method, we test it on various hazy images and compare with He *et al.*'s [29], Tarel*et al.*'s [46], Nishino *et al.*'s [49], and Meng*et al.*'s [50] methods. All the algorithms are implemented in the MatlabR2013a environment on a P4-3.3GHz PC with 6GB RAM. The parameters used in the proposed method are initialized as follows: r = 15, β = 1.0, θ0 = 0.121779,

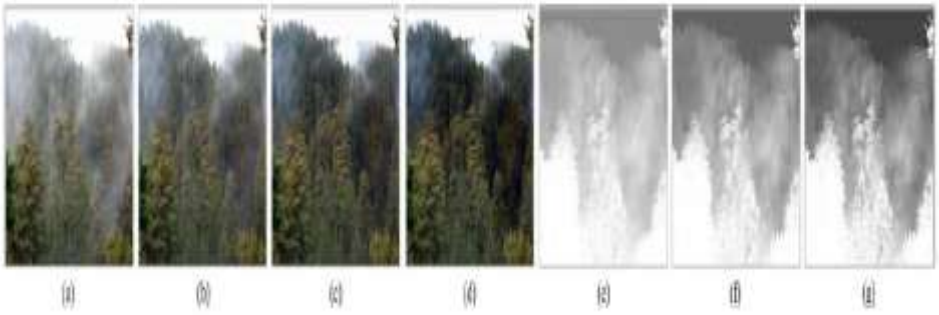

Fig. 11. Comes about with an alternate dispersing coefficient β. (a) The foggy picture. (b) The last outcome with β = 0.5. (c) The last outcome with β = 0.8. (d) The last outcome with β = 1.2. (e) The reestablished transmission outline β = 0.5. (f) The reestablished transmission outline β = 0.8. (g) Thereestablished transmission delineate β = 1.2.

Fig. 12. Qualitative comparison of different methods on real-world images. (a) The hazy images. (b) Tarel et al.'s results. (c) Nishino et al.'s results. (d) He et al.'s results. (e) Meng et al.'s results. (f) Our results.

θ1 = 0.959710, θ2 = −0.780245 and σ = 0.041337. For fair comparison, the parameters used in the four popular dehazing methods are set to be optimal according to [29], [46], [49], and [50].

10.1 Qualitative Comparison on Real-World Images

As all the dehazing calculations can get better than average outcomes by dehazing the general open air pictures, it is hard to rank them outwardly. Keeping in mind the end goal to think about them, we complete the calculations on some difficult pictures with extensive white or dark locales, since most existing dehazing calculations are not delicate to the white shading.

Figure 12 demonstrates the subjective correlation of results with the four cutting edge dehazing calculations [29], [46], [49], [50] on testing genuine pictures. Figure 12(a) delineates the cloudy pictures to be dehazed. Figure 12(b-e) demonstrates the consequences of Tarel et al. [46], Nishino et al. [49], He et al. [29], and Meng et al. [50], individually. The consequences of the proposed calculation are given in Figure 12(f). As appeared in Figure 12(b), the greater part of the dimness is expelled in Tarel's outcomes, and the points of interest of the scenes and items are very much reestablished. Be that as it may, the outcomes fundamentally experience the ill effects of over-improvement (for example, the sky locale of the principal picture is much darker than it ought to be, and the characteristics of the ladies in the last picture get to be distinctly cocoa). This is on account of Tarel's calculation depends on He et al's. calculation which has an innate issue of overestimating the transmission as examined in [29]. In addition, radiance curios show up close to the discontinuities in Figure 12(b) (see the mountain in the main picture and the leaves of plant in the second picture) because of that the "middle of the middle channel" utilized as a part of [46] is not an edge saving channel. The consequences of Nishino et al. have a comparable issue as Nishino et al's. calculation tends to over improve the neighborhood difference of the picture. As we can see in Figure 12(c), the reestablished pictures are oversaturated and mutilated, particularly in the third picture (the shade of the shirt is changed to dim).

Interestingly, the aftereffects of He et al are vastly improved outwardly (see Figure 12(d)). The thick dimness out yonder can be very much expelled, and there are no radiance antiquities. All things considered, shading twisting still shows up in the areas with white questions, for example, the shirt in the third picture. The reason can be clarified as takes after: As the technique for recuperating the transmission utilized as a part of [29] depends on the dull channel earlier, the precision of the estimation emphatically relies on upon the legitimacy of the dim channel earlier. Shockingly, this earlier is invalid when the scene splendor is like the barometrical light, and the evaluated transmission is hence not sufficiently solid at times. Furthermore, the air light is additionally a critical variable for figuring the transmission in [29]. Hence, keeping in mind the end goal to acquire the right transmission, a precise estimation of the environmental light is required. Notwithstanding, the approach for assessing the climatic light proposed by He et al. has its confinement and the assessed result is a rough esteem as talked about in [29]. Consequently, He et al's. calculation is inclined to overestimating the transmission.

International Journal of Research
Available at https://edupediapublications.org/journals
p-ISSN: 2348-6848
e-ISSN: 2348-795X
Volume 03 Issue 18
December 2016

Fig. 13. Comes about on stereo pictures where the ground truth arrangements are known. (a) The dim pictures. (b) Tarel et al's. results. (c) Nishino et al's. results. (d) He et al's. results. (e) Meng et al's. results. (f) Our outcomes. (g) Ground truth.

Meng et al's. results are near those got by He et al. as showed in Figure 12(e). This is because of the reality that,althoughMeng et al. enhance the DCP approach [29] by including a limit imperative, it doesn't address the issue of equivocalness between the picture shading and dimness.

Contrasted and the consequences of the four calculations, our outcomes are free from oversaturation. As showed in Figure 12(f), the sky and the cloud in the pictures are clear and the points of interest of the mountains are improved reasonably.

A. Qualitative Comparison on Synthetic Images

In Figure 13, the five calculations including the proposed one are tried on the stereo pictures where the ground truth pictures are known. Figure 13(a) demonstrates the foggy pictures which are combined from the fog free pictures with known profundity maps. The consequences of the five calculations are appeared in Figure 13(b-f). Figure 13(g) gives the ground truth pictures for examination. These fog free pictures and their comparing ground truth profundity maps are taken from the Middlebury stereo datasets [57]–[61]. Clearly Tarel et al's. results are very not quite the same as the ground truth pictures as the outcomes are much darker (see the toy with red hair in the dolls picture and the books in the books picture in Figure 13(b)).

By watching the pictures in Figure 13(c), we can find that Nishino et al's. results have a comparable issue. For instance, the shade of the toys in the dolls picture is changed into yellow, and the shade of foundation in the moebius picture is darker. He et al's. results are more like the ground truth pictures yet at the same time demonstrate a few errors (see Figure 13(d)). Take note of that the foundation in the books picture is darker than it ought to be. Essentially, Meng et al's. results additionally experience the ill effects of over-improvement as appeared in Figure 13(e). Clearly the shade of the veil in the cones picture is a long way from that in Figure 13(g). Interestingly, our outcomes don't have the issue of oversaturation and keep up the first shades of the items (see Figure 13(f)).

B. Quantitative Comparison

With a specific end goal to quantitatively evaluate and rate the calculations, we compute the mean squares blunder (MSE) and the basic closeness (SSIM) [62] of the outcomes in Figure 13 for correlation. The MSE of every outcome can be ascertained by the accompanying condition:

$$e = \sqrt{\frac{1}{3N} \sum_{c \in \{r,g,b\}} \|\mathbf{J}^c - \mathbf{G}^c\|^2}, \qquad (24)$$

International Journal of Research
Available at https://edupediapublications.org/journals
p-ISSN: 2348-6848
e-ISSN: 2348-795X
Volume 03 Issue 18
December 2016

where J is the dehazed picture, G is the ground truth picture, Jc speaks to a shading channel of J, Gcrepresents a colorchannel of G, N is the quantity of pixels inside the picture G, and e is the MSE measuring the contrast between the dehazed picture J and the ground truth picture G. Take note of that J and G have a similar size since they are comparing with the murky picture I. Given J and G, a low MSE speaks to that the dehazed result is fulfilling while a high MSE implies that the dehazing impact is not worthy.

TABLE I
TIME CONSUMPTION COMPARISON WITH HE *et al.* [29], TAREL *et al.* [46], NISHINO *et al.* [49], AND MENG *et al.* [50]

Image Resolution	He et al.'s method [29]	Tarel et al.'s method [46]	Nishino et al.'s method [49]	Meng et al. 's method [50]	Our method
441 × 450	9.866s	4.141s	91.661s	6.171s	**1.420s**
600 × 450	12.228s	8.229s	104.670s	4.468s	**2.219s**
1024 × 768	36.896s	69.294s	317.386s	10.231s	**4.278s**
1536 × 1024	73.571s	218.033s	649.722s	17.334s	**9.636s**
1803 × 1080	90.717s	351.139s	861.360s	21.567s	**12.314s**

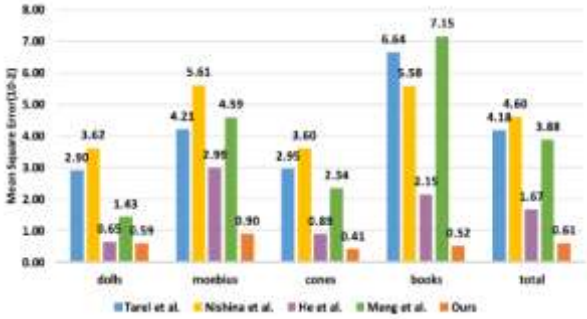

Fig. 14. Mean squared error (MSE) of different algorithms.

We also show the MSEs of the results made by different estimations in Figure 14. As can be seen,Nishino et al's. comes about make the most amazing MSEs as a rule. The high MSEs are basically in light of the over-change as said earlier. Tarel et al's. comes about beat Nishino et al's. in the underlying three pictures while they perform more frightful in the books pictures. Meng et al's. comes about rank third with respect to the total execution. The total MSE of He et al's. results is 0.0167, which is more than twice more diminutive than the other three. On the other hand, our system fulfills the most insignificant MSEs in all cases.

A. The collaborator similarity (SSIM) picture quality assessment list [62] knows about overview the capacity to save the basic data of the estimations. A high SSIM addresses high likeness between the dehazed picture and the ground truth picture, while a low SSIM passes on the regressive criticalness. Figure 15 displays the SSIM of the outcomes in Figure 13. The SSIMs of Nishona et al's. results are all lower than 0.7 exhibiting that much right hand data in the photographs has been lost. Tarel et al's. SSIMs look like those of Meng et al., however neither of them can go to 0.8. Clearly the SSIMs of He et al. are much higher than the other three in the four pictures. Our outcomes satisfy the most stunning SSIMs crushing the four figurings.

B. Complexity

International Journal of Research
Available at https://edupediapublications.org/journals
p-ISSN: 2348-6848
e-ISSN: 2348-795X
Volume 03 Issue 18
December 2016

Given a picture of size m ×n and range r , the multifaceted nature of the proposed dehazing calculation is just O(m×n×r), when the straight coefficients θ0, θ1, θ2 in Equation (8) are gotten. In Table I, we give the time utilization examination with He et al. [29] (quickened by the guided picture separating [43]), Tarel et al. [46], Nishino et al. [49], and Meng et al. [50].

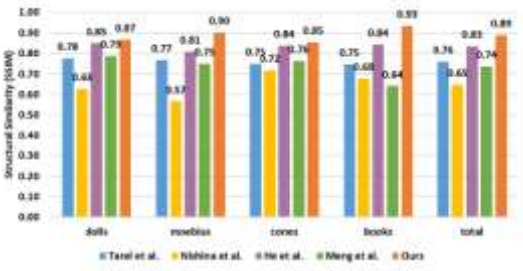

Fig. 15. Structural similarity (SSIM) of different algorithms.

As should be obvious, our approach is much speedier than others and accomplishes productive processing notwithstanding when the given murky picture is extensive. The high proficiency of the proposed approach for the most part advantages from the way that the direct model in view of the shading weakening earlier essentially improves the estimation of the scene profundity and the transmission.

OUTPUT

DISCUSSIONS AND CONCLUSION

In this paper, we have proposed a novel direct shading weakening earlier, in view of the contrast between the splendor and the immersion of the pixels inside the dim picture. By making a straight model for the scene profundity of the dim picture with this straightforward however intense earlier and taking in the parameters of the model utilizing an administered learning technique, the profundity data can be all around recouped. By method for the profundity delineate by the proposed technique, the scene brilliance of the dim picture can be recuperated effectively. Test comes about demonstrate that the proposed approach accomplishes drastically high effectiveness and remarkable dehazing impacts too. In spite of the fact that we have figured out how to display the scene profundity with the splendor and the immersion of the cloudy picture, there is still a typical issue to be understood. That is, the scrambling coefficient β in the barometrical diffusing model can't be viewed as a consistent in inhomogeneous environment conditions [55]. For instance, a district which is kilometers far from the

eyewitness ought to have a low estimation of β. Hence, the dehazing calculations which depend on the environmental diffusing model are inclined to belittling the transmission sometimes. As all the current single picture dehazing calculations depend on the consistent β suspicion, a more adaptable model is profoundly wanted. To beat this test, some more progressed physical models [63] can be considered. We leave this issue for our future research.

REFERENCES

[1] G. A. Woodell, D. J. Jobson, Z.-U. Rahman, and G. Hines, "Advanced image processing of aerial imagery," *Proc. SPIE*, vol. 6246, p. 62460E, May 2006.

[2] L. Shao, L. Liu, and X. Li, "Feature learning for image classification via multiobjective genetic programming," *IEEE Trans. Neural Netw. Learn.Syst.*, vol. 25, no. 7, pp. 1359– 1371, Jul. 2014.

[3] Zhu and L. Shao, "Weakly-supervised cross-domain dictionary learning for visual recognition," *Int. J. Comput. Vis.*, vol. 109, nos. 1–2, pp. 42–59, Aug. 2014.

[4] Y. Luo, T. Liu, D. Tao, and C. Xu, "Decomposition-based transfer distance metric learning for image classification," *IEEE Trans. ImageProcess.*, vol. 23, no. 9, pp. 3789–3801, Sep. 2014.

[5] Tao, X. Li, X. Wu, and S. J. Maybank, "Geometric mean for subspace selection," *IEEE Trans. Pattern Anal. Mach. Intell.*, vol. 31, no. 2, pp. 260–274, Feb. 2009.

[6] J. Han *et al.*, "Representing and retrieving video shots in human-centric brain imaging space," *IEEE Trans. Image Process.*, vol. 22, no. 7, pp. 2723–2736, Jul. 2013.

[7] J. Han, K. Ngan, M. Li, and H.-J. Zhang, "A memory learning framework for effective image retrieval," *IEEE Trans. Image Process.*, vol. 14, no. 4, pp. 511–524, Apr. 2005.

[8] Tao, X. Tang, X. Li, and X. Wu, "Asymmetric bagging and random subspace for support vector machines-based relevance feedback in image retrieval," *IEEE Trans. Pattern Anal. Mach. Intell.*, vol. 28, no. 7, pp. 1088–1099, Jul. 2006.

[9] Sensing images based on weakly supervised learning and high-level feature learning," *IEEE Trans. Geosci. Remote Sens.*, vol. 53, no. 6, pp. 3325–3337, Jun. 2015.

[10] Cheng *et al.*, "Object detection in remote sensing imagery using a discriminatively trained mixture model," *ISPRS J. Photogramm. RemoteSens.*, vol. 85, pp. 32–43, Nov. 2013.

[11] J. Han *et al.*, "Efficient, simultaneous detection of multi-class geospatial targets based on visual saliency modeling and discriminative learning of sparse coding," *ISPRS J. Photogramm. Remote Sens.*, vol. 89, pp. 37–48, Mar. 2014.

[12] L. Liu and L. Shao, "Learning discriminative representations from RGB-D video data," in *Proc. Int. Joint Conf. Artif. Intell.*, Beijing, China, 2013, pp. 1493–1500.

[13] Tao, X. Li, X. Wu, and S. J. Maybank, "General tensor discriminant analysis and Gabor features for gait recognition," *IEEE Trans. PatternAnal. Mach. Intell.*, vol. 29, no. 10, pp.1700–1715, Oct. 2007.

[14] Z. Zhang and D. Tao, "Slow feature analysis for human action recognition," *IEEE Trans. Pattern Anal. Mach. Intell.*, vol. 34, no. 3, pp. 436–450, Mar. 2012.

[15] T. K. Kim, J. K. Paik, and B. S. Kang, "Contrast enhancement system using spatially adaptive histogram equalization with temporal filtering," *IEEE Trans. Consum. Electron.*,vol. 44, no. 1, pp. 82–87, Feb. 1998.

[16] J. A. Stark, "Adaptive image contrast enhancement using generalizations of histogram equalization," *IEEE Trans. Image Process.*, vol. 9, no. 5, pp. 889–896, May 2000.

[17] J.-Y. Kim, L.-S. Kim, and S.-H. Hwang, "An advanced contrast enhancement using partially overlapped sub-block histogram equalization," *IEEETrans. Circuits Syst. Video Technol.*, vol. 11, no. 4, pp. 475–484, Apr. 2001.

[18] Y. Y. Schechner, S. G. Narasimhan, and S. K. Nayar, "Instant dehazing of images using polarization," in *Proc. IEEE Conf. Comput. Vis. PatternRecognit. (CVPR)*, 2001, pp. I-325–I-332.

[19] S. Shwartz, E. Namer, and Y. Y. Schechner, "Blind haze separation," in *Proc. IEEE Conf. Comput. Vis. Pattern Recognit. (CVPR)*, vol. 2. 2006, pp. 1984–1991.

[20] Y. Y. Schechner, S. G. Narasimhan, and S. K. Nayar, "Polarization-based vision through haze," *Appl. Opt.*, vol. 42, no. 3, pp. 511–525, 2003.

[21] S. G. Narasimhan and S. K. Nayar, "Chromatic framework for vision in bad weather," in*Proc. IEEE Conf. Comput. Vis. PatternRecognit. (CVPR)*, Jun. 2000, pp. 598–605.

[22] S. K. Nayar and S. G. Narasimhan, "Vision in bad weather," in *Proc. IEEE Int. Conf. Comput. Vis. (ICCV)*, vol. 2. Sep. 1999, pp. 820–827.

[23] S. G. Narasimhan and S. K. Nayar, "Contrast restoration of weather degraded images,"*IEEE Trans. Pattern Anal. Mach. Intell.*, vol. 25, no. 6, pp. 713–724, Jun. 2003.

[24] S. G. Narasimhan and S. K. Nayar, "Interactive (de) weathering of an image using physical models," in *Proc. IEEE Workshop ColorPhotometric Methods Comput. Vis.*, vol. 6. France, 2003, p. 1.

[25] J. Kopf *et al.*, "Deep photo: Model-based photograph enhancement and viewing," *ACM Trans. Graph.*, vol. 27, no. 5, p. 116, Dec. 2008.

[26] R. T. Tan, "Visibility in bad weather from a single image," in *Proc. IEEE Conf. Comput. Vis. Pattern Recognit. (CVPR)*, Jun. 2008, pp. 1–8.[27] R. Fattal, "Single image dehazing," *ACM Trans. Graph.*, vol. 27, no. 3,p. 72, Aug. 2008.

[27] P. S. Chavez, Jr., "An improved dark-object subtraction technique for atmospheric scattering correction of multispectral data," *Remote Sens.Environ.*, vol. 24, no. 3, pp. 459–479, Apr. 1988.

[28] K. He, J. Sun, and X. Tang, "Single image haze removal using dark channel prior," *IEEE Trans. Pattern Anal. Mach. Intell.*, vol. 33, no. 12, pp. 2341–2353, Dec. 2011.

[29] S.-C. Pei and T.-Y. Lee, "Nighttime haze removal using color transfer pre-processing and dark channel prior," in *Proc.*

19th IEEE Conf. ImageProcess. (ICIP), Sep./Oct. 2012, pp. 957–960.

[30] K. B. Gibson, D. T. Vo, and T. Q. Nguyen, "An investigation of dehazingeffects on image and video coding," *IEEE Trans. Image Process.*, vol. 12, no. 2, pp. 662–673, Feb. 2012.

[31] J. Yu, C. Xiao, and D. Li, "Physics-based fast single image fog removal," in *Proc. IEEE 10th Int. Conf. Signal Process. (ICSP)*, Oct. 2010, pp. 1048–1052.

[32] B. Xie, F. Guo, and Z. Cai, "Improved single image dehazing using dark channel prior and multi-scale retinex," in *Proc. Int. Conf. Intell. Syst.Design Eng. Appl.*, Oct. 2010, pp. 848–851.

[33] Q. Zhu, S. Yang, P. A. Heng, and X. Li, "An adaptive and effective single image dehazing algorithm based on dark channel prior," in *Proc.IEEE Conf. Robot. Biomimetics (ROBIO)*, Dec. 2013, pp. 1796–1800.

[34] Xiao and J. Gan, "Fast image dehazing using guided joint bilateral filter," *Vis. Comput.*, vol. 28, nos. 6–8, pp. 713–721, Jun. 2012.

[35] Y. Xiang, R. R. Sahay, and M. S. Kankanhalli, "Hazy image enhancement based on the full-saturation assumption," in *Proc. IEEE Conf.Multimedia Expo Workshops (ICMEW)*, Jul. 2013, pp. 1–4.

[36] Tomasi and R. Manduchi, "Bilateral filtering for gray and color images," in *Proc. 6th Int. Conf. Comput. Vis. (ICCV)*, Jan. 1998, pp. 839–846.

[37] S. Paris and F. Durand, "A fast approximation of the bilateral filter usinga signal processing approach," in *Proc. Eur. Conf. Comput. Vis.*, 2006, pp. 568–580.

[38] Porikli, "Constant time O(1) bilateral filtering," in *Proc. IEEE Conf. Comput. Vis. Pattern Recognit. (CVPR)*, Jun. 2008, pp. 1–8.

[39] Q. Yang, K.-H. Tan, and N. Ahuja, "Real-time O(1) bilateral filtering," in *Proc. IEEE Conf. Comput. Vis. Pattern Recognit. (CVPR)*, Jun. 2009, pp. 557–564.

[40] Adams, N. Gelfand, J. Dolson, and M. Levoy, "Gaussian KD-trees for fast high-dimensional filtering," in *Proc. ACM SIGGRAPH*, 2009, pp. 21:1–21:12.

[41] Adams, J. Baek, and M. A. Davis, "Fast high-dimensional filtering using the permutohedral lattice," *Comput. Graph. Forum*, vol. 29, no. 2, pp. 753–762, May 2010.

[42] K. He, J. Sun, and X. Tang, "Guided image filtering," *IEEE Trans. Pattern Anal. Mach. Intell.*, vol. 35, no. 6, pp. 1397–1409, Jun. 2013.

[43] Levin, D. Lischinski, and Y. Weiss, "A closed-form solution to natural image matting," *IEEE Trans. Pattern Anal. Mach. Intell.*, vol. 30, no. 2, pp. 228–242, Feb. 2008.

[44] J.-P. Tarel and N. Hautiere, "Fast visibility restoration from a single color or gray level image," in *Proc. IEEE 12th Int. Conf. Comput. Vis. (ICCV)*, Sep./Oct. 2009, pp. 2201–2208.

[45] J.-P. Tarel, N. Hautière, L. Caraffa, A. Cord, H. Halmaoui, and D. Gruyer, "Vision enhancement in homogeneous and heterogeneous fog," *IEEE Intell. Transp. Syst. Mag.*, vol. 4, no. 2, pp. 6–20, Apr. 2012.

[46] O. Ancuti, C. Ancuti, C. Hermans, and P. Bekaert, "A fast semiinverseapproach to detect and remove the haze from a single image," in *Proc. Asian Conf. Comput. Vis. (ACCV)*, 2010, pp. 501–514.

[47] L. Kratz and K. Nishino, "Factorizing scene albedo and depth from a single foggy image," in *Proc. IEEE 12th Int. Conf. Comput. Vis. (ICCV)*, Sep./Oct. 2009, pp. 1701–1708.

[48] K. Nishino, L. Kratz, and S. Lombardi, "Bayesian defogging," *Int. J. Comput. Vis.*, vol. 98, no. 3, pp. 263–278, Jul. 2012.

[49] Meng, Y. Wang, J. Duan, S. Xiang, and C. Pan, "Efficient image dehazing with boundary constraint and contextual regularization," in *Proc. IEEE Int. Conf. Comput. Vis. (ICCV)*, Dec. 2013, pp. 617–624.

[50] K. Tang, J. Yang, and J. Wang, "Investigating haze-relevant features in a learning framework for image dehazing," in *Proc. IEEE Conf. Comput.Vis. Pattern Recognit. (CVPR)*, Jun. 2014, pp. 2995–3002.

[51] L. Breiman, "Random forests," *Mach. Learn.*, vol. 45, no. 1, pp. 5–32, Oct. 2001.

[52] Q. Zhu, J. Mai, and L. Shao, "Single image dehazing using color attenuation prior," in *Proc. Brit. Mach. Vis. Conf. (BMVC)*, Nottingham, U.K., 2014, pp. 1–10.

[53] J. McCartney, *Optics of the Atmosphere: Scattering by Molecules and Particles*. New York, NY, USA: Wiley, 1976.

[54] S. G. Narasimhan and S. K. Nayar, "Vision and the atmosphere," *Int. J. Comput. Vis.*, vol. 48, no. 3, pp. 233–254, Jul. 2002.

[55] S. G. Narasimhan and S. K. Nayar, "Removing weather effects frommonochrome images," in *Proc. IEEE Conf. Comput. Vis. PatternRecognit. (CVPR)*, 2001, pp. II-186– II-193.

[56] Scharstein and R. Szeliski, "A taxonomy and evaluation of dense twoframe stereo correspondence algorithms," *Int. J. Comput. Vis.*, vol. 47, nos. 1–3, pp. 7–42, Apr. 2002.

[57] Scharstein and R. Szeliski, "High-accuracy stereo depth maps using structured light," in *Proc. IEEE Conf. Comput. Vis. PatternRecognit. (CVPR)*, Jun. 2003, pp. I-195–I-202.

[58] Scharstein and C. Pal, "Learning conditional random fields for stereo," in *Proc. IEEE Conf. Comput. Vis. Pattern Recognit. (CVPR)*, Jun. 2007, pp. 1–8.

[59] Hirschmüller and D. Scharstein, "Evaluation of cost functions for stereo matching," in *Proc. IEEE Conf. Comput. Vis. PatternRecognit. (CVPR)*, Jun. 2007, pp. 1–8.

[60] Scharstein*et al.*, "High-resolution stereo datasets with subpixel-accurate ground truth," in *Proc. German Conf. PatternRecognit. (GCPR)*, 2014, pp. 31–42.